AIAA JOURNAL
Vol. 30, No. 4, April 1992

Force Measurement on Rotating, Ablating Models Using an Air Bearing Balance

C. W. Haldeman* and A. D. Weinberg†
Massachusetts Institute of Technology, Lincoln Laboratory, Lexington, Massachusetts 02173

Test procedures and experimental results are presented for force measurements on rotating, ablating models of various materials in the NASA Ames Research Center 20-MW Aerothermal Facility utilizing a novel air bearing balance. The experiment attempted to document the functionality of the balance and quantify the magnitude of a spin induced side force resulting from a thermal phase lag on an ablating, conical model. It was determined that this force was less than 2.2% of the normal force, the experimental resolution. Normal force data plots demonstrate good agreement with theoretical inviscid predictions. Axial force is lower, as expected, and for high ablators, the center of pressure is slightly forward compared to nonablating models.

Nomenclature

A = model surface area
B = blowing parameter
B_m = molar blowing parameter
C_A = axial force coefficient
C_M = moment coefficient
$C_{m\alpha a}$ = out-of-plane moment coefficient slope due to ablation
C_N = normal force coefficient
C_Y = side force coefficient
F_A = axial force on model
F_N = normal force on model
F_Y = side force on model
M = Mach number evaluated at theoretical model center of pressure
$\dot{M}$ = mass ablation rate of model
m_{wall} = ablative material molecular weight
m_∞ = freestream molecular weight
q = dynamic pressure evaluated at theoretical model center of pressure
S = model base area
V = flow velocity
ρ = flow density

Introduction

FOR years, force measurement on models subjected to the high-enthalpy conditions of an arc heated wind tunnel has been a difficult, if not impossible, task. Strain gauge wind-tunnel balances, currently the most reliable instrument for force measurement in wind-tunnel environments, become adversely affected in arc heated flows because of their sensitivity to temperature transients and susceptibility to high electromagnetic interference (EMI). Recently, the Massachusetts Institute of Technology Lincoln Laboratory concluded tests using the NASA Ames 20-MW Aerothermal Facility, in which force data (normal force, side force, axial force, pitching moment, and yawing moment) were acquired on rotating, ablating models utilizing an innovative air bearing wind-tunnel balance.[1] This paper presents a detailed description of the balance and the results obtained with the balance when several ablating model materials (Teflon, epoxy, acrylic, carbon phenolic) and one nonablating material (ATJS graphite) were exposed to the arc heated flow. The Mach 7 flow was capable of producing true heating rate and enthalpy simulation for re-entry conditions that a body would experience at an altitude of 61 km and Mach number 22.

The complete run schedule inclusive of all testing parameters and model properties is presented in Tables 1 and 2. Where more than one run for each material was available for reduction, these data sets were all presented. Wherever applied, corrections to the data have been noted. Although some runs could not be completed due to loss of model through thermal shock loads, at least one model of each material tested, except carbon phenolic, provided data.

The NASA Ames tests were designed to verify the successful operation of the air bearing balance in the arc jet and to quantify the magnitude of aerodynamic forces present on slowly rotating (10 Hz or less), ablating, conical bodies. The forces sought included transverse forces (side forces) that might result when a symmetric body undergoes simultaneous rotation and ablation at angle of attack.[2,3] The test matrix of Table 1 was constructed to permit this force measurement as well as the usual in-plane forces and moments at the one flow condition of the test.

Data presented include normal force vs angle of attack, side force vs yaw angle, axial force vs yaw angle, and center of pressure vs yaw angle plots for the various materials.

Out-of-plane forces are not presented because they were smaller than the balance noise level. Although small pitch angle dependent side forces ($C_Y \approx 0.03$) were observed for some runs at spin rates of 2–10 Hz and were observed to reverse sign with spin, the results were neither consistent nor repeatable and could not be separated from balance errors.

Improvements in the balance or testing at a Reynolds number where the effect is larger will be required to measure the out-of-plane forces.

Air Bearing Balance

The balance used for the aforementioned measurements is notable because it utilized hydrostatic air bearings for both model support and force measurement. It was designed specifically for this test in order to overcome some difficulties usually encountered with strain gauge balances in this test environment.

The most significant drawback to the strain gauge balance is the coupling between mechanical stiffness and gauge sen-

Presented as Paper 90-1760 at the AIAA 16th Aerodynamic Ground Testing Conference, Seattle, WA, June 18–20, 1990; received Sept. 4, 1990; revision received March 16, 1991; accepted for publication July 9, 1991.

*Senior Staff, Aerospace Engineering Group, 244 Wood Street. Member AIAA.
†Assistant Staff, Aerospace Engineering Group, 244 Wood Street. Member AIAA.

Table 1 Run schedule

Model material	Number of shells tested		Angles tested, deg		Spin rates tested, Hz
	Pitch	Yaw	Pitch	Yaw	
Graphite	6	3	10, 4, 2, 0, −2, −4	6, 4, 2, −2, −4, −8	0, 4, 10
Teflon	6	2	10, 4, 2, 0, −2	6, 4, 2, 0, −2, −4, −8	0, 4, 10
Teflon with boron nitride tip	1	—	10, 4, 2, −2, −4	—	4
Epoxy	7	1	10, 8, 4, 2, 0, −2, −4	2, 0, −2, −4, −8	0, 4, 10
Acrylic	1	1	10, 4, 2, −2, −4	4, 2, −2, −4, −8	0, 4

Table 2 Tunnel conditions and model properties

Arc jet tunnel conditions	Models (conical)
8-deg conical nozzle	Heat shields: graphite, Teflon, epoxy, acrylic
Stagnation pressure P_0 (kPa) = 345.0	
Stagnation enthalpy H_0 (kJ/kg) = 17,445.0	
Sidewall calorimeter heat flux Q (kJ/m^{2}s) = 394.0[a]	Nose tips: graphite, boron nitride
Mach number M = 7.2[a]	Virtual length (cm) = 39.5
Dynamic pressure (kPa) = 3.4	Base area (cm)^2 = 45.5

[a]Evaluated at model center of pressure.

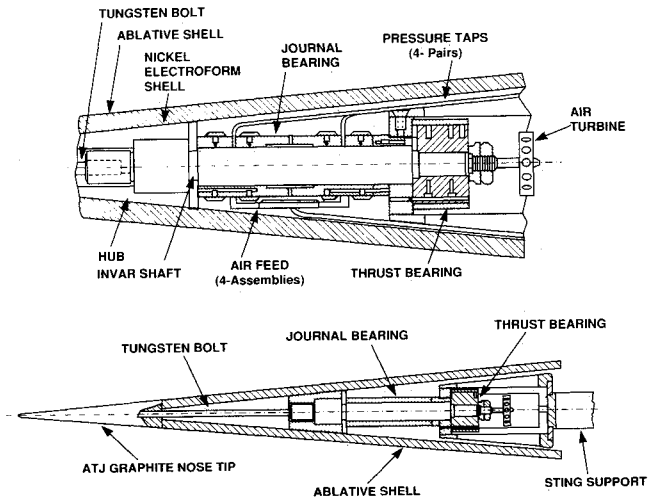

Fig. 1 Hydrostatic air bearing wind-tunnel balance.

sitivity. Any attempt to increase the load capacity of a strain gauge balance results in an increase in balance stiffness and a corresponding reduction in sensitivity. In fact, the limit of sensitivity is often dictated by the required stiffness to avoid static aeroelastic divergence of the balance.

Other drawbacks of the strain gauge balance include its sensitivity to electrical noise and ambient temperature. Arc jet tunnel environments where the local EMI is high or where temperature transients are present as a result of high or low operating temperatures are particularly severe.

Previous applications for air bearings have included supports for wind-tunnel test fixtures[4] and calibration components for specialized balance systems.[5] The air bearing balance represents an application that exploits the difference in hydrostatic film pressure across the bearing journal as a means of measuring the aerodynamic loads.

In this application, the supporting bearing uses a round shaft to provide rotational freedom for a spinning model. Alternative geometries, such as a square shaft, could be used where rotational freedom is not desired.

Principles of Operation

The hydrostatic gas bearing wind-tunnel balance consists of two hydrostatic journal bearings and a double acting thrust bearing, as shown in Fig. 1. The model shaft is supported in the pitch and yaw plane by the two journals and in the axial direction by the rear mounted double-acting thrust bearing. Aerodynamic loads are determined by measuring the differential hydrostatic film pressures between the support shaft and bearing surfaces. To measure forces on a rotating model, the shaft is round and free to rotate. Alternative designs could include restraint in roll with or without measuring rolling moment.

The forward and rear journals operate much like the forward and rear flexure pairs in a conventional balance. The difference in pressure between opposing pressure taps on a journal is a direct measure of the load on that journal acting along an axis through the pressure taps. Thus, the normal force is the sum of the loads on forward and rear journals, and the pitching moment is the difference of the forces multiplied by the length between journals. The force per unit pressure difference is not dependent on the overall pressurization level (to first order). The pressure difference developed by a given deflection of the shaft, however, is proportional to pressurization level. This fact provides for the basic separation of stiffness from sensitivity, which makes the air bearing balance different from the strain gauge balance. By using sensitive differential pressure transducers and operating at a high-pressure level, a balance can be made with both greater sensitivity and increased stiffness. Since it is possible for the shaft to make contact with a bearing surface without damaging the balance (at low spin rates), there is no possibility of the aeroelastic divergence problem, which often is the design limitation on strain gauge balances.

These advantages, however, are not obtained without corresponding disadvantages. There is the problem of the gas (nitrogen or air) injection into the wind-tunnel stream. The 28 l/min [standard ft^3/min (SCFM)] required for the balance could cause adverse aerodynamic effects in some cases. A second disadvantage is the relatively long time constant due to the high impedance of the small balance gap and relatively large volume associated with a pressure transducer and pressure tap line. To reach an asymptotic pressure value, 7 s were required.

Hardware and Fabrication

The gas bearings were designed using lubrication theory techniques.[6] The journal bearings were designed for a maximum load of 11.12 N (2.5 lbf) each for a total of 22.24 N (5 lbf), wheras the double acting thrust bearing was designed for a maximum load of 1.33 N (0.3 lbf).

The journal bearing shown in Fig. 2 is approximately 7.1 cm (2.8 in.) in length and 1.37 cm (0.54 in.) in diameter with a shaft diameter of 1.27 cm (0.500 in.). It contains four pairs of 0.018-cm-diam (0.007-in.) diametrically opposed pressure taps

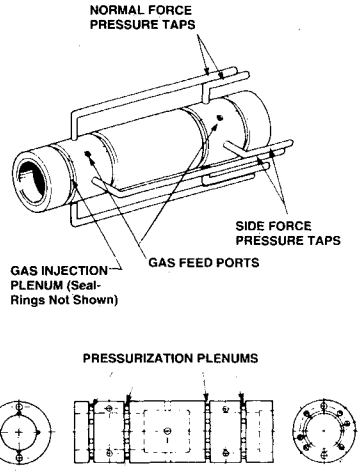

Fig. 2 Journal bearing: exterior view and cutaway.

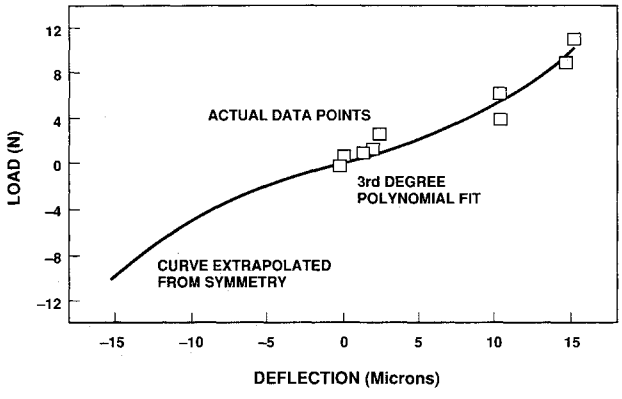

Fig. 3 Typical air bearing deflection curve.

and two sets of 16 0.018-cm-diam (0.007-in.) gas injection holes. Each tap is situated in the middle of four feed holes to provide a balanced bleedoff from the individual journal flow of 2.83 l/min (0.1 SCFM). The film collapse that pressure taps can cause in viscous air bearings cannot occur in the present geometry because it is not possible for the four metering holes to bleed off the entire support film from 16 injection holes.

Clearances are small, with the diametrical clearance between shaft and journal being nominally 0.003 cm (0.0012 in.). This results in a relatively stiff support. A load-deflection characteristic curve was made by reflecting a laser beam off a mirror on the balance shaft. This is shown in Fig. 3. The load of 10.7 N (2.4 lb) at a deflection of 0.0015 cm (0.0006 in.) corresponds to a stiffness of 14,020 N/cm (8000 lb/in.) for the two journals. The corresponding angular stiffness in pitch for the 5.08-cm (2-in.) journal separation is 1581 N-cm (140 in.-lb)/deg. At a feed pressure of 689.5 kPa (100 psi) (twice that of Fig. 3), the stiffness would be doubled.

The thrust bearing, shown in Fig. 4, is approximately 1.98 cm (0.78 in.) in length and 2.86 cm (1.125 in.) in diameter. It is mounted at the rear of the journal and provides axial support for the model shaft. It is double acting, tolerating both thrust and drag, and uses eight 0.013-cm-diam (0.005-in.) feed intake holes and eight 0.041-cm-diam (0.016-in.) pressure tap holes located on each face. Flow is approximately 25.5 l/min (0.9 SCFM), with a 25% bleedoff tolerance for film pressure measurement. Unlike the journal bearing, which has its pressure taps situated directly in the bearing surface, the thrust bearing has opposing internal plenums that, when pressurized from the 16 tap holes, provide an average measurement around the bearing perimeter. Experience with this design suggests that this bearing should have performed better with a much larger annular area. This would have reduced the 25.5-l/min (0.9-

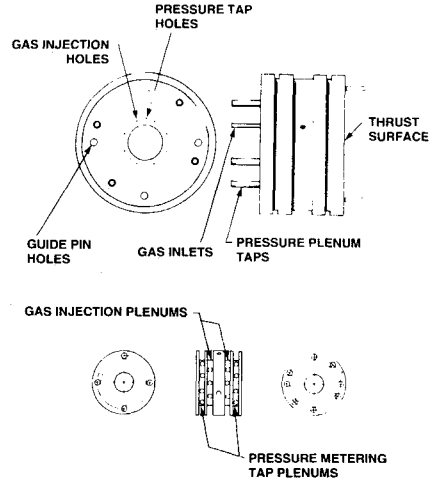

Fig. 4 Thrust bearing: exterior view and cutaway.

SCFM) flow and increased the maximum axial load capacity but at the cost of reduced sensitivity. With a differential pressure of 137.90 kPa (20 psi) at 0.0015-cm (0.0006-in.) deflection, the axial stiffness is computed at 5783 N/cm (3300 lb/in.).

Balance components were fabricated by Speedring Inc., Huntsville, Alabama, with a 1.27-μm (50-μin.) tolerance and 0.05-μm (2-μin.) surface finish. Hard naval brass was chosen (in retrospect, hard stainless steel would have been better) for both bearings due to its machinability, friction, and thermal properties. The model shaft was fabricated from Invar because of its low thermal expansion rate and was plasma sprayed with a coating of aluminum oxide to provide a hard polished surface. Calculations indicated that a temperature of 700°C (1752°R) would be required for the shaft to thermally expand and fill the available bearing clearance.

Spin Turbine

To provide model spin, a precision air turbine was constructed. The turbine, containing 13 separate impulse vanes, was affixed to the aft section of the model shaft behind the thrust bearing. A brass housing containing two sets of nozzles to drive the model in either a clockwise or counterclockwise direction was mounted over the turbine assembly and very carefully aligned to minimize force contributions. These electroformed nozzles were contoured to provide uniform Mach 2 airflow to the impingement surfaces. Spin rate was measured using an optical tachometer and recorded with the data acquisition personal computer.

Precision in fabrication and assembly allowed continuous operation of the air driven turbine with negligible tare introduction.

Operational Experience

A high level of air supply cleanliness was required. Infiltration of particles larger than 5 μm (197 μin.) cannot only cause friction but can also close up gas intake and/or pressure tap holes, thereby causing errors in film pressure measurements. Dry nitrogen filtered to 1 μm (39 μin.) was ultimately used as the pressurizing gas. Nevertheless, it was crucial to check balance cleanliness before each calibration and test. A large shift in model tares was usually indicative of a need for cleaning with Freon 113. Once clean, several weeks to a month between cleanings was possible.

As previously mentioned, a feature of the balance was the large time constant associated with reading the film pressures. The time required for an asymptotic reading was approximately 7 s. Whereas this is an advantage when averaging signals at constant test conditions, rapid pressure changes cannot be followed. If better time response is desired, future balance designs could include fiber optic position sensors to replace the current pressure taps. These optical sensors would provide

instantaneous measurement with some possible loss in sensitivity.

Balance drift was observed to be, at most, 5 mV of the 1000-mV transducer full range over a time of 90 min. This corresponds to 0.34 kPa (0.05 psi) over the ±68.94-kPa (10-psi) transducer range. Tests indicated that the drift was attributable to the transducers and not the gas bearing.

Calibration

Each journal was calibrated separately in the normal and side planes to help quantify respective load-pressure characteristics. A typical calibration is shown in Fig. 5.

Symmetry and linearity (at lower loads) was observed in both normal and side force calibrations of the journal bearing. What would appear to be calibration scatter of 1% full scale occurs under certain loading conditions in both force planes. As a result of this scatter, no improvement was noted by using the full interaction matrix calibration, and so a linear fit to the calibration data was applied and used in data reduction.

The exact cause of this scatter under certain loading conditions is not understood at the present time. A small spin/normal force interaction term is a possible cause. A modified journal geometry with four axial slots separating the four air pad locations is being examined. This geometry should exhibit reduced sensitivity but greatly reduce cross coupling effects of spin. It should also produce better calibration linearity while reducing scatter.

The thrust bearing calibration showed the bearing to be linear at and above its rated load capacity. This additional load was achieved by increasing the bearing's gas supply pressure above the design value. It is interesting to note that the thrust bearing did not exhibit the calibration scatter effect. Possible explanations include differences in flow venting and in supporting pressure film geometries between the two bearings.

Balance center was determined as that load point where both front and rear journal differential pressures in the normal plane increased by the same amount under load, i.e., the point about which no moment was generated. Moments were applied by hanging loads at different locations along the shaft using a calibration canister assembly. All calibrations were performed with a rotating shaft. This was necessary because it was found that the pressure readings varied by as much as 0.89 kPa (0.13 psi) with shaft angular position. This essentially provided a measure of eccentricity of the shaft. A spinning shaft averages out the effects due to this eccentricity. Figure 6 shows balance force data for a typical run. Data were recorded at a 50-Hz rate and averaged over 1 s. The force data plot clearly shows the asymptotic time response characteristics of the balance after 7 s. The lower portion of the side force plot displays the standard deviation of each 1-s sample. Standard deviation during the run was 0.013 N, indicating a signal-to-noise ratio on the order of 100. Given the conditions of the arc jet environment, this ratio is quite acceptable and demonstrates the sensitivity of the balance under adverse test conditions.

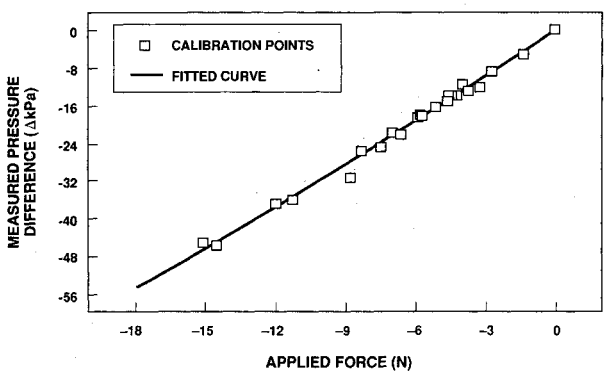

Fig. 5 Typical calibration curve: pitch plane, forward journal.

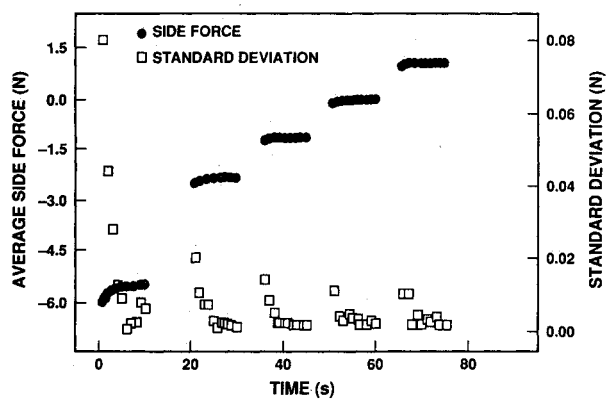

Fig. 6 Average side force vs time.

Test Configuration

Figure 7 shows the test configuration used in the NASA Ames facility. Models were positioned 3.6 cm (1.4 in.) downstream of the nozzle exit plane. The nozzle contour was conical with an 8-deg half-angle and a 30.5-cm (12.0-in.) exit diameter. All models were mounted to the air bearing balance, which was supported by a variable pitch, air actuated sting. The sting was mounted on an *x-y* traversing mechanism for movement of the whole assembly in or out of the arc heated flow and for establishing axial position. All instrumentation and metering lines from the balance/sting assembly were routed down through the water cooled, copper sting arm and out through an aluminum interface plate for connection to control and monitoring hardware. These systems included an air turbine assembly for spinning the model, an optical tachometer for measuring model spin rate, balance pressurization and metering lines, sting pressurization lines, and model pitch/yaw angle transducers. These transducers determined which of a series of step positions the model occupied. This stepping system had been shown by reflected laser calibration to be within ±0.02 deg. All electrical connections passing into or out of the interface plate required isolation to protect test personnel and equipment from possible high-voltage discharges that might be produced during arc heater startup. Model base pressure was also measured using systems already present in the NASA Ames facility.

Equipment for control and monitoring of all balance and sting systems within the wind tunnel was designed and fabricated for the test. This was contained in a single cabinet and provided regulated flow to the air bearing balance while also housing highly sensitive Datametrics (590-10D-2P1-V1R-4D ±10 psi pressure transducer, Edwards Datametrics Inc., Wilmington, Massachusetts) differential pressure transducers for measuring balance film pressures. All test data were recorded using an IBM AT personal computer equipped with an 8-channel, 16-bit analog-to-digital converter. The computer also automated the functions of data acquisition and sting control.

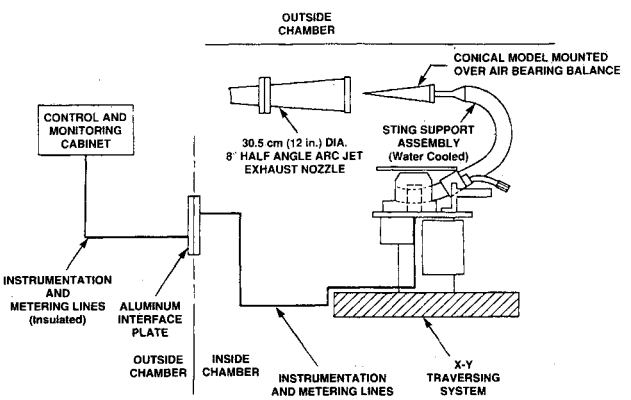

Fig. 7 Test configuration.

Test Procedure

Prior to exposure of a model to the flow, a 7.6-cm-radius (3.0-in.) combination impact pressure/calorimeter probe and a 5.5-deg half-angle conical, sidewall calorimeter were inserted into the flow to measure run conditions and to check on flow repeatability. The model was brought up to the desired spin rate using the air turbine instrumentation, and initial balance tares were then taken with the data acquisition computer. When all required test conditions were met, i.e., correct spin rate, entry pitch, or yaw angle, instrument display check, the model was traversed into the flow and positioned on the centerline. After a final verification of all systems and run parameters, the personal computer data acquisition program was actuated, automating the data collection and sting control sequencing for the duration of the run.

For runs with ATJS graphite models (a low ablator), balance temperature was carefully monitored to prevent excessive heating and damage to the balance. Thermocouples attached to critical sections of the balance were monitored to determine if a run needed to be prematurely terminated by removal of the test rig from the flow.

Following the completion of a run, final balance tares were taken. These tares, combined with balance normal force data and model weights, were used to determine the mass ablation rate of each model material for calculation of the blowing parameter.

Results

Flow Quality

Before any models were exposed to the flow, a survey with a 7.6-cm-radius (3.0-in.) impact pressure probe/calorimeter was performed. This was necessary because the facility's 8-deg half-angle conical nozzle typically produces a slightly expanding flow. Axial flow gradients were found to be the following: Mach number gradient = 0.032/cm (0.473%/cm) or ±9.4% over model length, and dynamic pressure gradient = 54.33 Pa/cm (1.14%/cm) or ±23.0% over model length. These gradients were significant over the 39.54-cm (15.58-in.) virtual model length. To extract average coefficients, all quantities were evaluated at the theoretical model center of pressure (67% of model virtual length referenced from apex).

In reducing the data from a single run of several points sequentially taken at increasing angles of incidence, it was found necessary to apply an angle-of-attack correction in the usual manner to produce the required symmetry about zero. These varied from 0.5 to 1.5 deg and were attributed to variable back pressure of the arc jet's vacuum system combined with the nonsymmetrical blocking effects of the model sting support and traversing mechanism. No similar effects were present in the yaw plane, and so yaw plane data were used for center of pressure determination.

Force Data

Figures 8 and 9 show typical force data for four models of differing material. Blowing parameters, calculated from the average mass loss, are given in Table 3. The symmetry of these plots demonstrates the utility of the air bearing balance in the harsh environment of the 20-MW arc jet and indicates that the flow can be useful for aerodynamic as well as thermal testing. Both plots show good agreement at small angles of attack with theoretical values tabulated in the Naval Surface Weapons Center inviscid cone tables[7] and exhibit divergence at the higher angles of attack where viscous effects are contributing. It is interesting to note the larger scatter (approximately 0.48% full scale) of the normal force coefficient vs angle-of-attack plot compared to the scatter (approximately 0.24% full scale) of the side force coefficient vs yaw angle plot. This larger scatter can be attributed to variations in flow angle combined with traversing system deflection and unpredictability of the time-dependent weight tare due to ablation. Corrections for flow angle and model tare weight were implemented

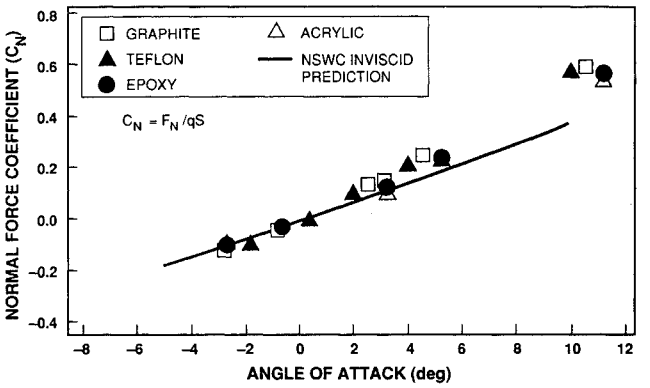

Fig. 8 Normal force coefficient vs angle of attack.

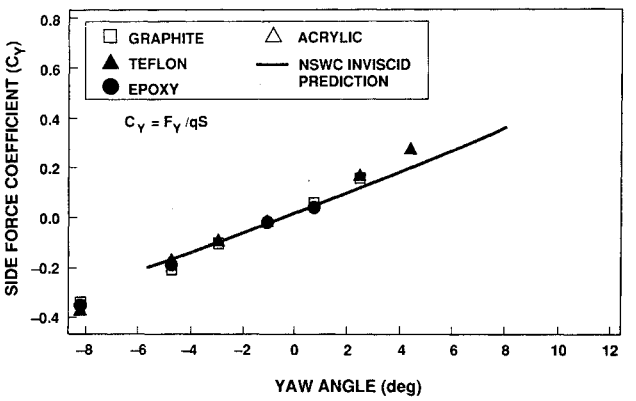

Fig. 9 Side force coefficient vs yaw angle.

for the data in Fig. 8. The side force coefficient vs yaw angle data in Fig. 9 were not corrected because flow angularity was very small in this plane.

Figure 10 demonstrates the balance's ability to measure axial force on various ablating shells. Axial force was corrected to an equivalent model base pressure equal to freestream static pressure. These corrections were small (less than 1% full scale). It is interesting to observe that epoxy and acrylic, the two ablators with the largest blowing parameters, experienced a lower axial force coefficient (approximately 60%) than the less ablative materials. This effect was expected because mass addition to the boundary layer tends to reduce the skin friction on the model.

In Table 3, the average blowing parameters, as determined from model weight loss, are listed along with assumed molecular weights and the molar blowing parameter, which corrects for ablator molecular weight (the 0.5 power is used from similarity arguments). In terms of the molar blowing parameter, one would expect the effect of Teflon to be much smaller than the other materials. Thus, the fact that the Teflon axial force appears slightly higher instead of slightly lower than graphite is not significant and is probably indicative that the axial force measurement error is of this order.

Figure 11 shows model center of pressure locations with yaw angle. All center of pressure locations occurred forward of the theoretical 67% virtual cone length (all locations were shifted farther toward the model nose) and little distinction can be made among ablators. Although center of pressure data are

Table 3 Model blowing parameters

Blowing parameter B, $B = \dot{M}/\rho AV$	Molar blowing parameter B_m, $B_m = B\sqrt{m_\infty/m_{wall}}$
B (Teflon) = 0.0094	B_m (Teflon) = 0.0051 (m_{wall} = 95)
B (epoxy) = 0.0202	B_m (epoxy) = 0.0181 (m_{wall} = 35)
B (acrylic) = 0.0144	B_m (acrylic) = 0.0186 (m_{wall} = 17)

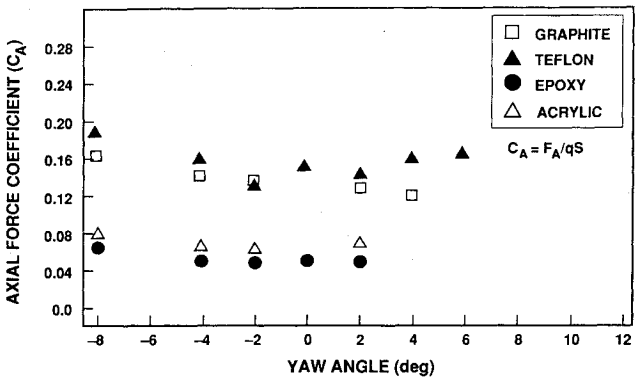

Fig. 10 Axial force coefficient vs yaw angle.

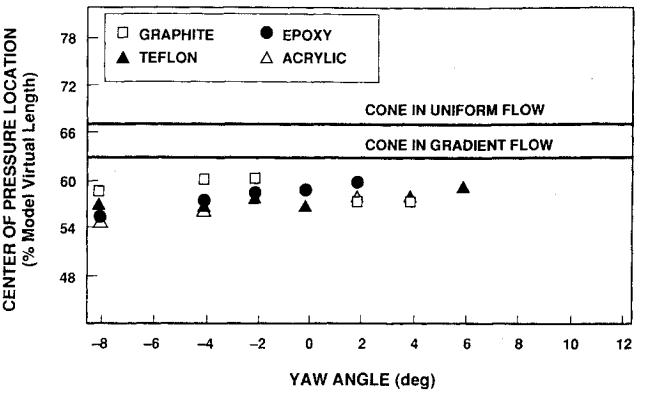

Fig. 11 Model center of pressure location vs yaw angle.

somewhat scattered, it appears that the higher blowing ablators have a location slightly forward of that for the nonblowing graphite shell.

Figure 11 also shows center of pressure locations for a cone in both a uniform and a gradient flow, predicted using Newtonian theory. The measured locations were farther forward (approximately 7% of virtual length) than predicted values for gradient flow. Since the nonablating graphite model also exhibited a center of pressure forward of that expected in the gradient flow, it appears that another mechanism, in addition to blowing, is operating to displace the center of pressure. This could be real gas relaxation behind the initial shock wave, causing pressures (and heat transfer) to be higher relative to ideal gas calculations near the nose and relaxation toward equilibrium values near the base.

Because of the sensitivity of the center of pressure calculation to errors in force and moment measurement particularly close to zero angle of attack, data from yawing runs were used for the reduction because, as mentioned, side plane data exhibited less scatter. Force coefficient and moment coefficient were corrected to remove offsets at zero angle of attack before computing center of pressure position from C_M/C_N. At zero angle of attack, moment and force coefficient slopes were used to avoid division by zero.

System Error Analysis

Total system error was determined from four separate sources: 1) calibration scatter, 2) tunnel dynamic pressure variation, 3) model base area variation due to ablation, and 4) side force scatter with varying angle of attack.

Scatter in the balance calibration was apparent before testing commenced, but its source is not known at present. It may be related to the details of the balance geometry and the close tolerances associated with the design of the air bearings. Since a resulting uncertainty of 1.1% full-scale normal force due to calibration scatter would still permit resolution of normal and side plane forces of interest, the test was conducted without resolving this point. No scatter in the balance's axial force calibration was present, although sensitivity was lower than that for normal force.

Variation in tunnel dynamic pressure resulted from small changes in arc and tunnel operating parameters. A 1.14% error due to the variation was calculated. This was the standard deviation of individual run conditions from the average.

Model shape change (base area considered only) was expected for those cones constructed of ablatable material. Posttest data reduction revealed an error in force coefficient of 1.44% from this source.

Small interaction in side force during model pitch was not expected prior to test commencement. This cross plane interaction was believed to result from inadequate stiffness in the tunnel's traversing support rig, coupled with a dependency on model spin direction. There was also a small residual swirl in the flow from the arc heater. The residual error from both of these effects was approximately 0.6%. The root sum square error from these sources was 2.2%.

Spin Induced Side Force

The test objective of quantifying the magnitude of a spin induced side force during model ablation was not realized, except to determine that it was smaller than the 2.2% experimental error. Whereas some individual runs showed small side force values increasing with angle of attack, these are not attributed to aerodynamic sources because there was no consistency from run to run, and side force was also present with the nonablating, graphite model. The most likely causes of this systematic error were deflection of the *x-y* traversing table or a previously undetected small, spin dependent side force-normal force balance interaction. The side plane data did not reveal repeatable distinctions among an ablating, spinning model; a nonablating, spinning model; an ablating, nonspinning model; or a nonablating, nonspinning model. Although for some runs a small side force was observed that reversed sign with spin direction, this was not dependent on ablation, being present for the graphite model as well. Thus, the most likely cause is the interaction mentioned earlier.

A spin induced side force would have had to be greater than 0.44 N (0.1 lbf) or a side force coefficient of 0.03 (the limit of the balance's side force resolution given a system error of 2.2%) to be detectable.

This result does enable some comparison with the theoretical results of Waterfall[2] and Tabibzadeh.[3] The level of out-of-plane moment assumed in Ref. 2 ($C_{m\alpha d}$ normal slope due to ablation $= -0.05$) to explain effects observed in flight would produce a moment coefficient $C_m = -0.007$ at an 8-deg angle of attack. This is 14% of the in-plane coefficient of ($+0.05$) and is clearly outside the balance error band and therefore measurable. The fact that this moment was not detected supports the results of Ref. 3, which predicted less than a 1% effect under conditions of the test due to thermal phase lag alone.

It is therefore suggested that the flight effects observed in Ref. 2 that occurred at much lower altitudes (≈ 30 km) than the test (≈ 60 km) were a result of a unique combination of the blowing with boundary-layer separation or transition where the asymmetrical blowing could cause asymmetry in boundary-layer separation (blowoff) or transition. Such fluid dynamic amplification of the effect could explain why it is large only at certain altitudes. This suggests that further tests at lower altitude conditions covering the flight range could clarify the phenomenon.

Conclusions

The results from the NASA Ames aerothermal tests show distinctive normal and axial force characteristics among conical ablatable materials in the arc heated flow. As expected, those models having higher ablation rates (epoxy, acrylic) experienced a lower axial force (approximately 60% less)

because skin friction was reduced through ablation. Only small differences in center of pressure location were present among the model materials.

As would be expected, normal force coefficient variations with angle of attack and side force coefficient variations with yaw angle measurements were relatively insensitive to ablation of differing materials. Both plots showed good agreement at small angles of attack with inviscid flow predictions.

Although a side force resulting from a spinning, ablating model was not measured, the testing did provide an upper limit to the magnitude of this force under the conditions of the test. Its value must be less than the root sum square of error introduced from the balance and arc jet facility hardware. Calculations indicate that the side force must measure less than 2.2% of full scale, i.e., the side force coefficient is less than 0.03 for all materials tested. Since no difference in forces and moments between models with a graphite tip (catalytic) and boron nitride tip (noncatalytic) could be detected, it is believed that wall catalytic effects were not important under the test conditions.

The ability to obtain useful force data in the harsh environment of an arc jet represents a significant step in high-enthalpy ground testing. The air bearing balance appears particularly well suited to certain areas of testing where its advantages can be exploited. These are the following: 1) arc tunnels where electrical noise and thermal drift are present, 2) cryogenic tunnels where thermal problems are severe, 3) magnus testing where high spin rate and great transverse sensitivity are required, and 4) gas injection testing where the air bearing support can read forces without physical connections carrying the injected gas. The flexible tubes or bellows that normally bridge the balance flexures can be eliminated.

Acknowledgments

This work was sponsored by the Department of the Air Force. The authors would like to thank William A. Figueiredo, currently with TRW Corporation, for his detailed design of the air bearing; Stanley Gray of Mechanical Technology, Inc., Latham, New York, who served as a consultant, and the many staff members at the NASA Ames Research Center 20-MW Aerothermal Facility who assisted with the testing.

References

[1]Haldeman, C. W., and Weinberg, A. D., "Some Initial Results With An Air Bearing Wind Tunnel Force Balance," AIAA Paper 90-1760, June 1990.

[2]Waterfall, A. P., "Effect of Ablation on the Dynamics of Spinning Re-Entry Vehicles," *Journal of Spacecraft,* Vol. 6, No. 9, 1969, pp. 1038–1044.

[3]Tabibzadeh, R., "Force and Thermal Effects on Rotating Ablating Bodies," M.S. Thesis, Massachusetts Inst. of Technology, Aeronautics and Astronautics Dept., Cambridge, MA, Jan. 1988.

[4]Regan, F. J., and Krumins, M. V., "Hypersonic Dynamic Testing of Ablation Models with Three Degree of Freedom Gas Bearings," *Journal of Spacecraft,* Vol. 20, No. 5, 1983, pp. 470–476.

[5]Vlajinac, M., "A Pneumatic Calibration Rig for Use with a Magnetic Suspension and Balance System," Massachusetts Inst. of Technology Aerophysics Lab., ARL Rept. 70-0016, Cambridge, MA, Jan. 1970.

[6]Grassam, N. S., and Powell, J. W., *Gas Lubricated Bearings,* Butterworths, London, 1964, pp. 110–267.

[7]Morrison, A. M., Solomon, J. M., Ciment, M., and Ferguson, R. E., "Handbook of Inviscid Sphere-Cone Flow Fields and Pressure Distributions," Naval Surface Weapons Center, White Oaks Lab., Rept. NSWC/Wol/Tr 75-45, White Oaks, MD, Dec. 1975.